NISTIR 6108

High-speed Temporal Characterization and Visualization of Spatial Light Modulators and Flat-panel Displays

Eung G. Paek
C. L. Wilson
J. W. Roberts
C. I. Watson
Information Technology Laboratory

U.S. DEPARTMENT OF COMMERCE
Technology Administration
National Institute of Standards and Technology
Gaithersburg. MD 20899-0001

NIST

High-speed Temporal Characterization and Visualization of Spatial Light Modulators and Flat-panel Displays

Eung G. Paek
C. L. Wilson
J. W. Roberts
C. I. Watson
Information Technology Laboratory

U.S. DEPARTMENT OF COMMERCE
Technology Administration
National Institute of Standards and Technology
Gaithersburg, MD 20899-0001

January 1998

High-speed Temporal Characterization and Visualization of Spatial Light Modulators and Flat-panel Displays

Eung G. Paek, C. L. Wilson, J. W. Roberts, and C. I. Watson

Information Technology Laboratory
National Institute of Standards and Technology (NIST), Gaithersburg, MD 20899

Abstract - An apparatus that can characterize and visualize temporal dynamics of spatial light modulators (SLM) and flat-panel displays is constructed and evaluated using a commercially available spatial light modulator. The apparatus is based on the stroboscopic video sampling method and has a temporal resolution on the order of microseconds, permitting measurement of a long event (> 100 ms) with a high signal-to-noise ratio. Experimental results demonstrate the visualization of the temporal image sequencing and addressing in an SLM.

To be submitted to Optics Letters

The spatial light modulator (SLM) has been widely used for optical information processing, pattern recognition, optical computing, holographic storage and displays [1]. The SLM has a finite response time (typically 1ms to 100 ms) depending on materials and addressing schemes. In the normal matrix addressing scheme, two-dimensional (2-D) information is loaded line-by-line from top to bottom, causing a time skew. These finite response times and time skews can cause serious problems, especially in coherent optical information processing, because the entire two-dimensional data must be present in the light path while processing is in progress[2-4]. The loaded information should not vary during information processing or during holographic recording. Also, all of the data of the prior frames must disappear before processing a new frame of data. For such temporal measurements of locally varying behavior of high speed SLM's (such as ferroelectric liquid crystal SLM's or deformable mirror devices), a high-speed, 2-D imaging apparatus is needed that can take a series of pictures with a time interval of sub-microseconds to cover the entire settling time of about 100 ms until a stable image is obtained.

To our knowledge, no previous work has been reported on the visual characterization of rapidly varying local behavior of 2-D SLM's. Conventional spot checks performed at each pixel are time-consuming and do not provide information on overall image evolution. Although high-speed photography using streak cameras or frame cameras can be used to take pictures with a sub-microsecond temporal resolution, it is expensive and complicated to use. Moreover, streak cameras can cover only a limited number of frames (typically about 10 frames at a time). Also, current high-frame-rate charged coupled devices (CCDs) cannot reach beyond several thousand frames per second. Recently, a low-cost method of capturing fast repetitive processes has been developed by Moller and Bruns [5]. The method is based on the conventional oscilloscopic sampling method applied to video images, as in a stroboscope.

In this Letter, we apply the low-cost video sampling method to characterize and visualize the rapidly varying SLM images and answer several important issues concerning the speed of an SLM. Figure 1 shows a schematic diagram of our apparatus: Light from a HeNe laser is focused by lens L_1 and is modulated by an acousto-optic modulator (AOM) (TeO_2 shear mode, NEOS model no. N23080) [6] to generate a light pulse with a pulsewidth of approximately 50 ns. Light from the AOM is collimated by lens L_2 and illuminates the SLM under test and subsequently forms an image at the output CCD plane using lenses L_3 and L_4. The spatial filter at the focal plane of lens L_3 blocks all higher-order diffracted beams originating from the grid structure of the SLM and passes only the 0-th order diffracted beam. This avoids spurious Moire fringing noise in the output images.

To accurately synchronize light pulses with SLM images, a precise timing relationship must be maintained between the pulse applied to the AOM and the video signal. In our case, a series of image patterns is generated by a frame grabber (EPIX, model no. SVIP-4MEG) and the video images are displayed repeatedly. The NTSC video signal is then converted to a VGA signal by a video-to-VGA converter and is loaded on the SLM under test. A sharp, strong pulse is added at the beginning of the series of images as a reference mark. The vertical sync signal from the converter and the reference mark generates a stable reference signal. The reference signal is delayed by a delay generator (Stanford Research Systems, model DG535) [6]. The delay generator has very fine resolution (5 ps) and a long range of delays up to 1000 s. The delayed pulse is mixed with a rf frequency and is loaded onto the AOM. Also, the output CCD is externally synchronized with the VGA signal through the sync signals from the converter. A

stationary stroboscopic image is detected by a CCD and is captured by a digital video recorder.
After each capture of an image, the time delay is increased incrementally by a desired amount to
take a sequence of pictures with controlled delay that sample the whole image sequence. The
images thus recorded for the entire event are displayed at normal speed, as for slow motion
videos. A conventional active matrix twisted nematic liquid crystal SLM for projection display
is used as a sample in this experiment.

Figure 2 shows the output intensity at two different points (**A** and **B** marked in the figure) at
the output CCD plane (separated by 12 ms) as a function of time delays. An image (letter "3") is
loaded twice (even and odd frames) in 1/30 s as in conventional NTSC video signals. At each
point in the output plane, light intensity increases to approximately half the peak values by the
first pulse of applied voltage and continues to increase up to the peak values by the second pulse.
The output is a convolution of two impulses separated by 1/60 s and the temporal impulse
response of the liquid crystal in the linear region of the CCD. The two curves show similar
tendencies but the first one obtained at point **A** shows less intermediate plateauing. This
difference is attributed to the non-uniformity of light intensity illuminating the SLM. Both curves
reach peaks after 27 ms and decay in 10 ms.

In Figure 3, a series of SLM images taken every 4 ms shows dynamic evolution of the
images. A series of input images (the numbers 1, 2, 3, and 4) is presented repeatedly at video
rate. Each input image lasts for 1/30 s (interlaced) and blank images are added before and after
the numbers to allow measurement of writing and decay time without being interrupted by
neighboring images. The delay times are measured with respect to the loading of the first pixel

(on the left top corner) of the first image "1". The first image appears from top to bottom until a full image is revealed after 28 ms. The second image begins to appear before the first image decays and the two images overlap for about 24 ms (from 40 ms to 64 ms). A reasonably isolated image appears only for 8 msec before the next image begins to overlap. The intermediate transition of images from one to the other and the resultant crosstalk is evident in the pictures.

For high temporal resolution, the pulsewidth of illuminating light needs to be short. In this case, contrast of an acousto-optic modulator is one of the most important parameters and is related to the signal-to-crosstalk ratio (SCR) of an output image by

$$\text{SCR} = \frac{\Delta t}{T} \times \text{CR}, \tag{1}$$

where Δt, T and CR refer to pulsewidth, duration of total event, and contrast ratio of the optical switch, respectively. The AOM used in this experiment has a contast ratio of approximately 4,000 (measured) to permit $T = 4000 \, \Delta t$ for SCR=1.

Another important parameter as pulsewidth becomes narrower is the intensity of the light illuminating the SLM (I) which is related with the minimum detectable light intensity of a CCD (S) as

$$I \times \frac{\Delta t}{T} \times L \geq S, \tag{2}$$

where L is the sum of insertion losses from AOM, SLM, and other optical components. The minimum detectable intensity of the CCD used in this experiment (Pulnix, model TM-7EX)[6] is

approximately $0.01~\mu W/cm^2$ at the HeNe wavelength of 633 nm. When the light level is weak, the integration (averaging) method can be used to compensate for the reduced SCR, as in conventional sampling oscilloscopes.

The bulky laser and the acousto-optic modulator used in this experiment can be replaced by a high-power, pulsed laser diode or a light emitting diode (LED) to make the system both compact and inexpensive. In addition, the laser diode can have better contrast ratio than an AOM due to its threshold nature. Also, a high-speed LED can be used for better images without speckle noise.

In conclusion, we have constructed a stroboscopic video sampling system to characterize and visualize the temporal dynamics of SLM's and certain kinds of flat-panel displays such as liquid crystals displays or deformable mirror devices. The system was used to visually characterize active-matrix twisted-nematic liquid crystal displays, which turned out to be unsatisfactory for real-time video-rate processing. The use of the system for other displays, including an array of self-luminous smart pixels, is currently being investigated.

Acknowledgment

References :

1. *Spatial light modulator technology, materials, devices and applications*, edited by U. Efron, Marcel Dekkar, Inc. New York, 1994.

2. D. Casasent and C.L. Wilson, "Optical metrology for industrialization of optical information processing," NIST-IR 6060, Sept. 1997.

3. J.C. Kirsch, D. Gregory, M.W. Thie and B.K. Jones, "Modulation characteristics of the Epson liquid crystal television," Opt. Eng. 31 (5), pp. 963-970, 1992.

4. C. Soutar, S.E. Monroe and J. Knopp, "Measurement of the complex transmittance of the Epson liquid crystal television," Opt. Eng. 33 (4), pp. 1061-1068, 1994.

5. M. Moller and H.-J. Bruns, "Video sampling: a new low-cost method of capturing fast repetitive process," SPIE vol. 2549, pp. 2-11, 1995.

6. Certain commercial equipment or components are identified in this paper only to specify the experimental procedure adequately. Use of these equipment or components does not constitute an endorsement by NIST or any other agency of the Department of Commerce.

Figure Captions:

Figure 1. Schematic diagram of a system for stroboscopic temporal characterization and visualization of SLM's.

Figure 2. Output intensities at two different points at the output plane (marked with "A" and "B" and are separated by 12 ms in time with each other) as a function of time delays. An image (letter "3") is loaded twice (even and odd frames) in 1/30 sec.

Figure 3. Temporal development of a series of images loaded on a typical active matrix twisted nematic liquid crystal SLM. A series of images (the numbers 1, 2, 3, and 4) are presented at video rate, and blank images are added before and after the numbers to show writing and decay of the images. The snapshot images are taken every 4 ms, and the delay times are measured with respect to the initial loading of the first pixel (on the left top corner) of the first image "1".
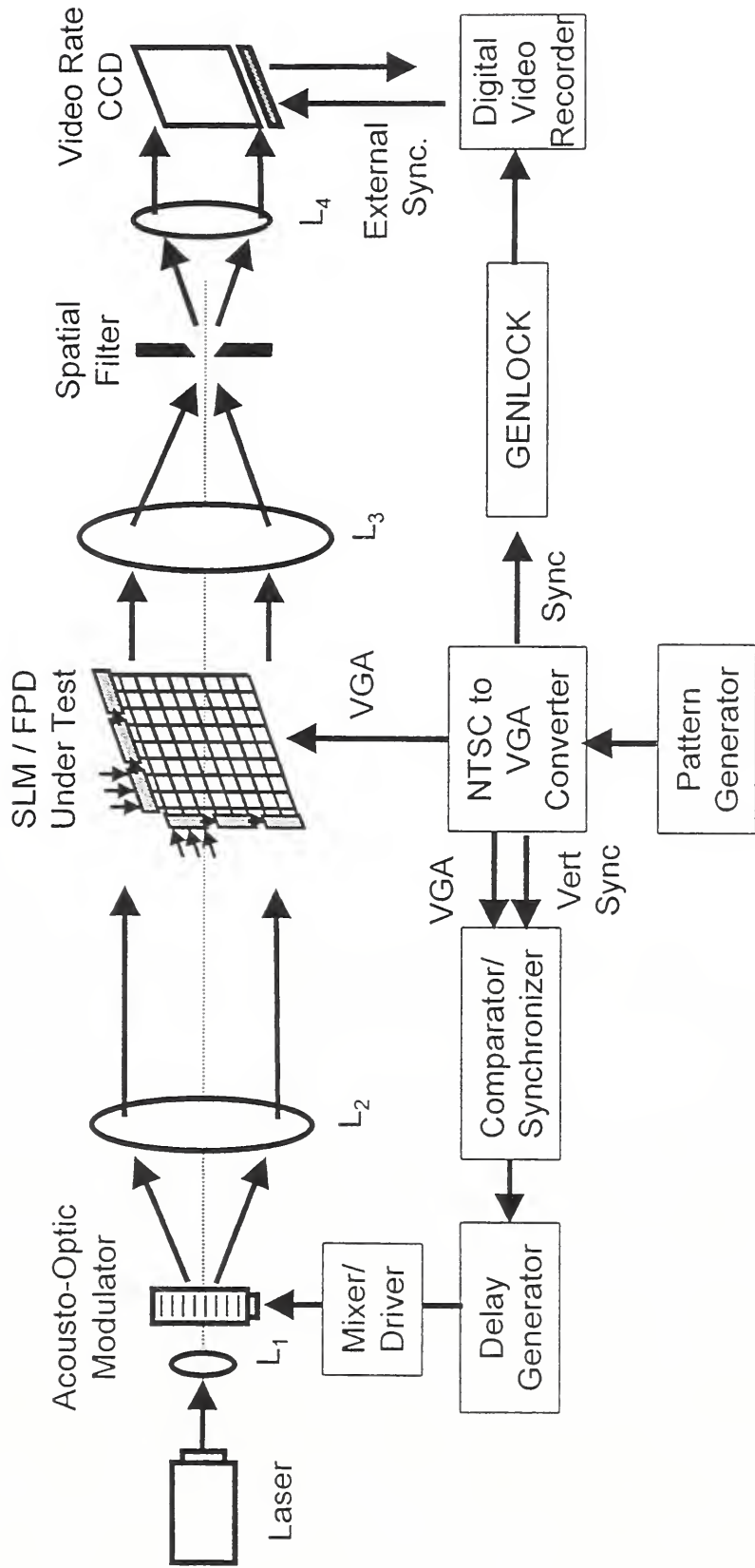
Figure 1. Schematic diagram of a system for stroboscopic temporal characterization and visualization of SLMs.
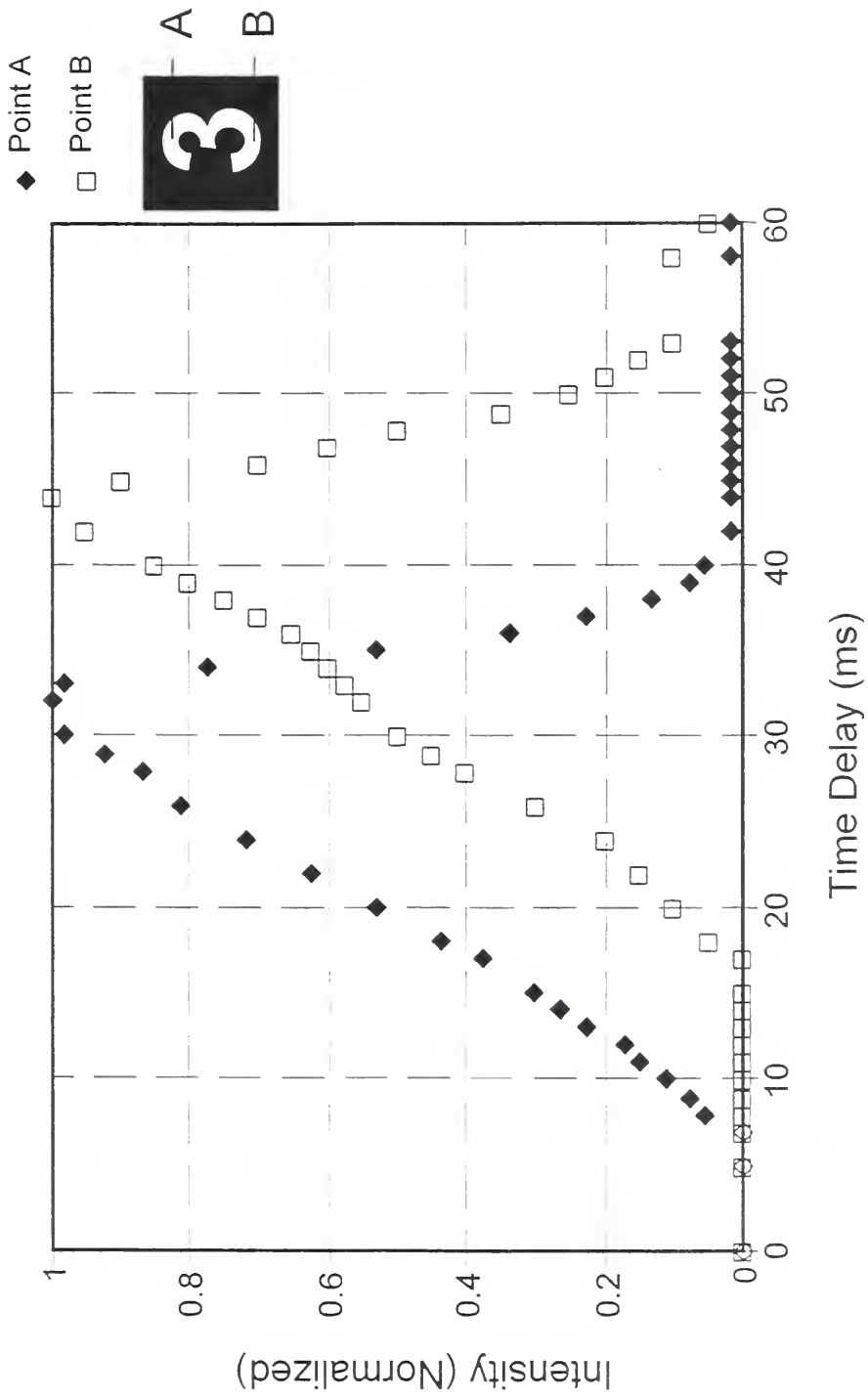
Figure 2. Output intensities at two different points at the output plane (marked with "A" and "B" and are separated by 12 ms in time) as a function of time delays. An image (letter "3") is loaded twice (even and odd frames) in 1/30 sec.
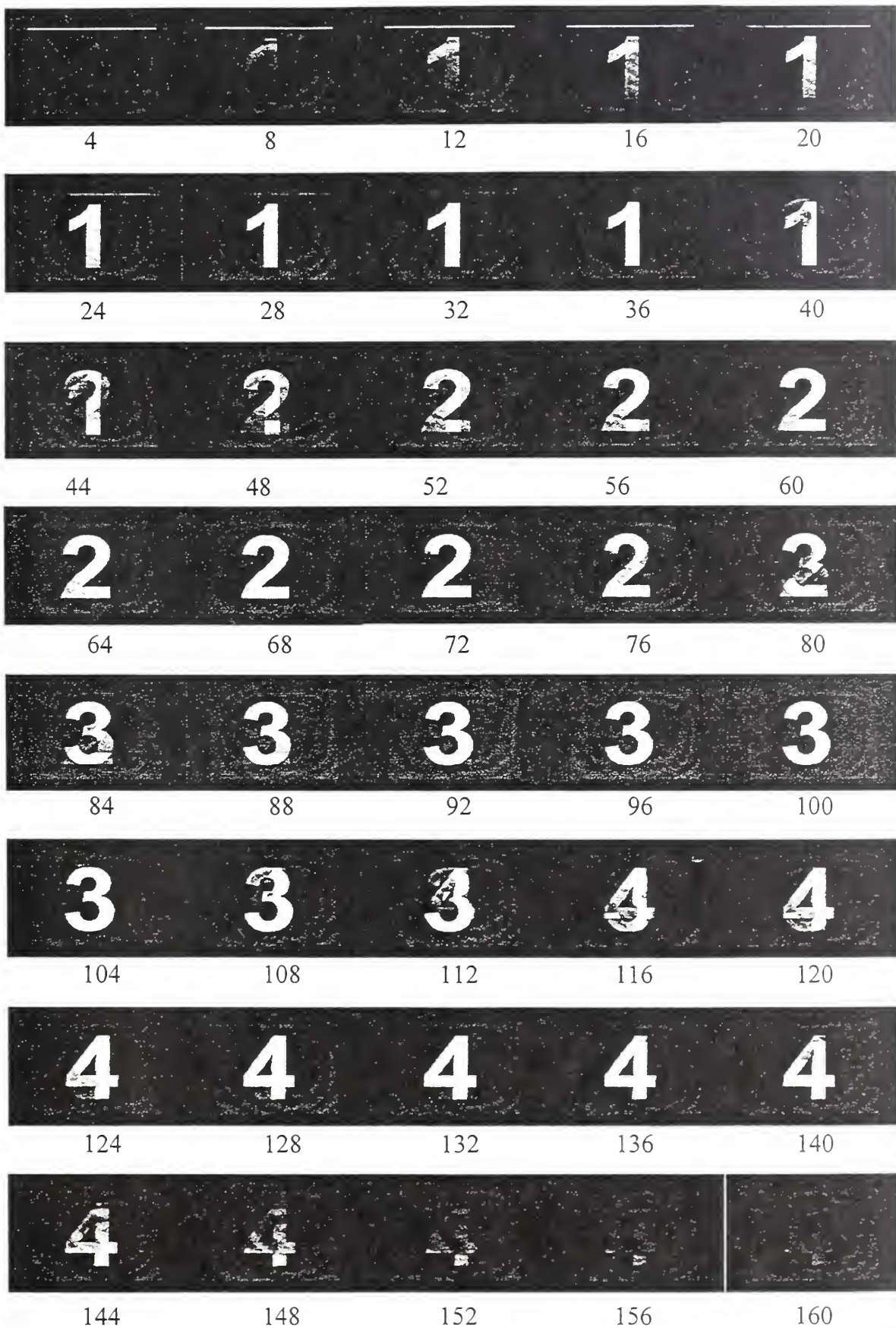
4	8	12	16	20
24	28	32	36	40
44	48	52	56	60
64	68	72	76	80
84	88	92	96	100
104	108	112	116	120
124	128	132	136	140
144	148	152	156	160

Figure 3.